Relationship between aggregate microstructure and mortar expansion. A case study of deformed granitic rocks from the Santa Rosa mylonite zone

Hans-Rudolf Wenk · P. J. M. Monteiro · K. Shomglin

Abstract It is shown that the deformation state of a granitic rock has a profound impact on the long-term stability of concrete, if used as aggregate due to enhanced susceptibility to the alkali-silica reaction. An investigation of the microstructure of granitic rocks from the Santa Rosa mylonite zone in southern California with transmission electron microscopy and neutron diffraction revealed that, as these rocks become progressively deformed from granite to mylonite and phyllonite, accompanied by grain size reduction, the dislocation density in quartz (investigated with TEM) increases and preferred orientation of biotite (determined by neutron diffraction) becomes stronger. While the contribution of dislocations to the bulk energy increase of quartz is low, dislocations provide favorable sites for dissolution and precipitation to occur. A comparison with ASTM C 1260 expansion tests of these same samples indicates that expansion increases with the dislocation density.

Introduction

The alkali-silica reaction (ASR) involves reactive siliceous minerals in aggregates and highly alkaline concrete pore solutions producing an expansive alkali-silicate gel, which can imbibe water and then expand. Many dams, reinforced concrete bridges, and pavements require continuous repair or replacement because of cracks caused by this deleterious reaction. Concrete deterioration caused by the ASR has been investigated for many years, however, an understanding of the mechanisms underlying this expansion is still limited. Compounding this problem is that deformed silicates are easily available and often used as aggregates for concrete, but there is no reliable test to characterize their potential reactivity. It is recognized that the deformation state, grain size, and development of foliation in granitic rocks used as aggregate in concrete influence the alkali-silica reaction [1–6]. By performing an analysis of preferred orientation in conjunction with expansion tests, Monteiro et al. showed [6] that there is a quantitative relationship between the degree of deformation and reactivity in granitic rocks. However, to further understand the cause of differing levels of susceptibility of quartz in deformed rocks to the alkali-silica reaction, we have analyzed the microstructure of deformed quartz by transmission electron microscopy.

In this article, we will characterize microstructural features, by transmission electron microscopy (TEM), observing dislocations and determining dislocation densities of quartz grains in granitic rocks of different deformation states. These results are then compared with expansion tests of concrete, for which the same rocks have been used as aggregate.

H.-R. Wenk (✉) · K. Shomglin
Department of Earth and Planetary Science, University of California, 307 McCone Hall, Berkeley, CA 94720-4767, USA
e-mail: wenk@berkeley.edu

P. J. M. Monteiro
Department of Civil and Environmental Engineering, University of California, Berkeley, CA 94720-4767, USA

Materials

The rocks used for testing were obtained from the Santa Rosa mylonite zone in southern California. The mylonite zone lies on the eastern edge of the Peninsular Ranges batholith and was pervasively deformed in a ductile regime

shortly after the emplacement of the batholith in the late Cretaceous. The mylonite zone extends over 30 km and is 200 m to 1.5 km wide and strains are very large as evaluated from a study of enclaves [7]. Granite deformed to mylonite at the outer margin of the batholith. Locally within the mylonite, extremely deformed areas of phyllonite and ultramylonite developed that are best exposed in upper Palm Canyon, south of Palm Springs. Previous studies quantified the processes that occurred during the transformation of granite to mylonite and phyllonite, particularly, the development of preferred orientation, and the evolution of microstructure [8–10].

Granite samples are identified as PC 89 and PC 715, mylonite samples are PC 82, PC 708, PC 709, PC 714, and PC 720, and the phyllonite samples are PC 92 and PC718. The localities are listed in Table 1.

Granite samples PC 89 and PC 715 consist of approximately 27% quartz, 52% plagioclase, 6% orthoclase, and 8% biotite. The rock is medium to fine grained and is holocrystalline. Anhedral quartz and plagioclase is abundant, biotite is subsidiary. Quartz grain size ranges from 0.1 to 3 mm, biotite from 0.05 to 1.5 mm, and feldspar 0.25 to 2.5 mm. The results of mild deformation can be seen by the presence of undulatory extinction of quartz (Fig. 1a). Some areas of the rock showed a fine-grained mixture of quartz and biotite resulting from grain-size reduction due to deformation. This matrix comprises less than 25%. Although the samples have experienced some deformation, it is not sufficient to produce foliation or significant preferred orientation of mineral components.

Table 1 Classification and location of each sample, as well as percentage of fine-grained matrix

Sample name	Classification	Location	Matrix (%)
PC 89	Granite	116°30′37″ W, 33°35′10″ N	<10
PC 715	Granite	116°34′30.5″ W, 33°34′31″ N	25
PC 82	Mylonite	116°30′02″ W, 33°35′06″ N	70
PC 708	Mylonite	116°28′17.5″ W, 33°34′36″ N	50
PC 709	Mylonite	116°28′21″ W, 33°34′36″ N	55
PC 714	Mylonite	116°28′25″ W, 33°34′34″ N	70
PC 720	Mylonite	116°30′16″ W, 33°35′ N	75
PC 92	Phyllonite	116°31′15″ W, 33°34′54″ N	99
PC 718	Phyllonite	116°30′12″ W, 33°34′50″ N	97
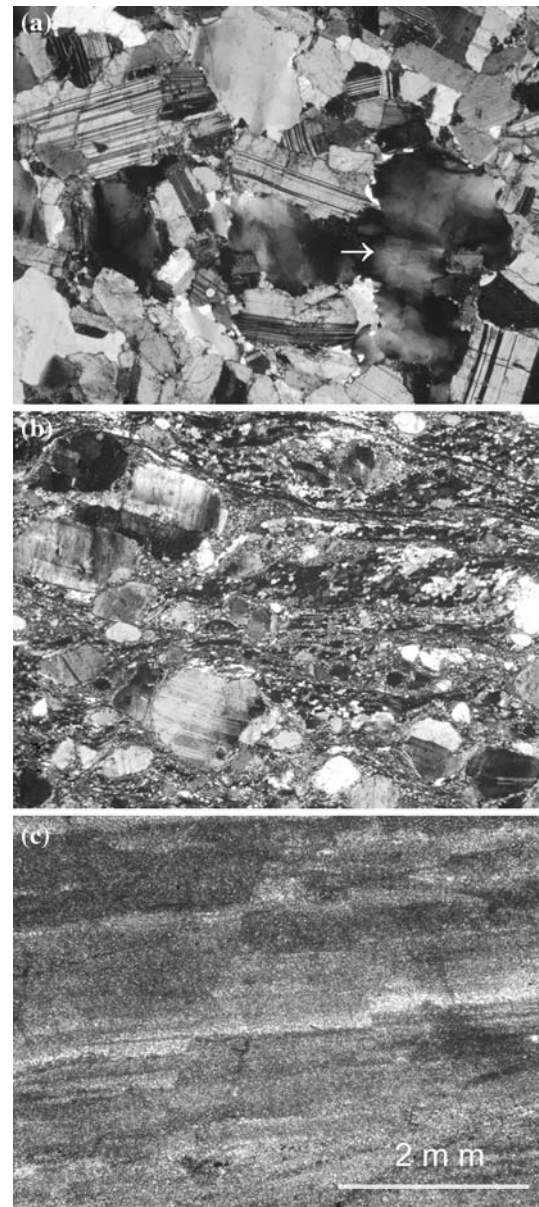
Fig. 1 Micrographs of samples taken with a petrographic microscope, crossed polars. All images have same magnification. (**a**) Granite (PC 89) contains the largest mineral grains out of the three classifications. The effects of mild deformation can be seen in the undulatory extinction of quartz (shown by the arrow). (**b**) Mylonite (PC 82) shows an overall grain size reduction of quartz, biotite, and to some extent feldspar due to deformation. Compositional layering of the mineral develops. (**c**) Phyllonite (PC 92), experiencing the greatest degree of deformation and grain size reduction, contains no grains visible to the unaided eye

Mylonite samples PC 82, PC 708, PC 709, PC 714, and PC 720 have undergone more deformation, matrix content is higher, and the overall grain size is lower. Quartz grain size ranges from 0.05 to 1 mm, biotite from 0.05 to 1 mm, and feldspar from 0.1 to 3 mm. There are large clasts, mainly of feldspar and a fine-grained matrix. The matrix

content ranges from 50 to 75%. In addition, compositional segregation begins to develop, leading to a layered foliation (Fig. 1b). Reduction of grain size is accompanied by recrystallization. Lineation, the alignment of minerals along a certain direction, is also seen in these samples. There was not enough material of PC 82 to perform expansion tests and thus, the texturally analogous sample PC 714 was used.

Phyllonite samples PC 92 and PC718 are most strongly deformed with the largest percentage of matrix and the smallest grain size. Phyllonite samples are brown gray rocks with visible foliation and lineation. No crystals can be seen with the unaided eye (Fig. 1c). With the use of a microscope, a few remaining feldspar clasts are seen. Feldspar grain size ranges from 0.05 to 0.15 mm, quartz and biotite grains are no larger than 30 μm, and the rock contains 95% matrix. Preferred orientation of the minerals is present [10].

Chemical compositions of the rock samples were obtained by using X-ray fluorescence (XRF). The results of these analyses are listed in Table 2. Mineral content of each rock was calculated from its chemical composition by means of the C.I.P.W. norm [11], and is listed in Table 3. Although there are minor variations in both the chemical and mineralogical composition, composition is similar and corresponds to granite/granodiorite. Both the oxide weight % and mineral weight % show no systematic change with increasing deformation. It will be assumed that any change in reactivity from sample to sample is not caused by differences in chemical or mineralogical composition.

Experimental methods

Transmission electron microscopy

From samples selected for analysis, 30 μm thin sections were prepared without the attachment of a cover slip. Crystal Bond instead of epoxy was used as the binding agent. Individual grains or areas containing quartz were selected, and cut with a razor blade. Then thin sections are heated until the Crystal Bond begins to melt, and the selected areas were removed. After cleaning with acetone, the areas of interest were mounted onto a copper hexagonal grid with general-purpose epoxy and then ion-thinned.

Brightfield images of dislocations in quartz were taken using a JEOL 200CX scanning transmission electron microscope at the National Center for Electron Microscopy (NCEM) at the Lawrence Orlando Berkeley Laboratory (LBL). This instrument is equipped with a side-entry double-tilt goniometer stage. The microscope was operated at 200 kV in TEM mode for all samples. Images were collected on film, and developed on-site.

Expansion test

ASTM C 1260 is a standardized test used by cement chemists, concrete technologists, and industry to rapidly determine the susceptibility of a rock to the alkali-silica reaction [12]. The rocks to be used in this test are crushed down to sand-size, and graded to the specification listed in the test. An aggregate/cement ratio of 2.25 and a water–cement ratio of 0.45-0.47 (by mass) is used. Enough mortar is mixed to make three mortar bars with the dimensions of 25 × 25 × 285 mm. The mortar bars were cured for 24 h in a fog room at 23 ± 1.7 °C, de-molded, and immersed in water in a closed container. The container is then placed in a water bath maintained at 80 °C. After 24 h, the length of the specimens was measured, and then immersed in a closed container of 1 M sodium hydroxide solution maintained at 80 °C. The volume of the hydroxide solution is 3.5–4.5 times the volume of the mortar bars. Periodically, the specimens were removed briefly from the containers and measured before significant cooling occurred. The average expansion of the three mortar bars after 14 days of immersion in the hydroxide solution is used to estimate the reactivity of the aggregate. Generally, a 0.0–0.1% expansion means that the specific aggregate tested is not reactive, 0.1–0.2% is considered to be inconclusive and requires

Table 2 Chemical composition of major elements obtained by XRF analysis of rock samples collected from the Santa Rosa mylonite zone

Oxide % by weight	NaO_2	MgO	Al_2O_3	SiO_2	K_2O	CaO	FeO
PC 89 granite	3.87	1.40	17.01	64.68	1.85	4.46	2.20
PC 715 granite	3.33	1.67	16.70	63.80	4.26	4.26	5.78
PC 708 mylonite	2.38	0.16	13.37	75.34	6.16	1.35	0.70
PC 709 mylonite	3.21	0.46	14.23	71.91	4.60	1.92	2.59
PC 714 mylonite	3.52	0.50	14.87	72.31	2.83	3.78	3.27
PC 720 mylonite	3.19	1.22	14.80	68.70	2.82	3.01	1.83
PC 92 phyllonite	3.76	1.47	16.72	64.06	1.94	4.77	2.23
PC 718 phyllonite	3.43	1.17	15.94	66.63	2.83	3.44	4.37

Table 3 Mineralogical composition computed through the use of the C.I.P.W. standard norm from the chemical composition (Table 2)

Mineral % by weight	Quartz	Orthoclase	Albite	Anorthite	Biotite	Magnetite
PC 89 granite	27.2	6.0	33.4	18.7	8.1	2.4
PC 715 granite	23.4	15.8	24.7	15.1	11.4	7.3
PC 708 mylonite	29.5	39.7	22.2	6.7	0.7	0.1
PC 709 mylonite	27.6	25.1	28.1	8.2	5.0	3.9
PC 714 mylonite	28.7	15.3	32.1	14.2	4.3	2.9
PC 720 mylonite	27.7	11.9	28.0	15.6	8.6	4.9
PC 92 phyllonite	26.1	6.6	32.5	19.8	7.8	3.3
PC 718 phyllonite	32.8	16.0	24.6	11.0	7.5	3.2

further testing, and greater than 0.2% is considered to be reactive.

Neutron diffraction and data analysis

Neutron diffraction texture analysis relied on two methods: old data for samples PC 82, PC 89, and PC 92, measured with monochromatic radiation on diffractometer D1B at Institut Laue Langevin in Grenoble [9] were reanalyzed with modern methods [13]. New measurements on the rest of the samples were performed with the time-of-flight (TOF), High-Pressure Preferred Orientation (HIPPO) neutron diffractometer at the Los Alamos National Laboratory, Los Alamos Neutron Science Center (LANSCE), and Manuel Lujan Jr. Neutron Scattering Center [14].

Samples for measurement were prepared from oriented hand specimens of rock. Cores with a diameter of 9 mm and a height of 12 mm were taken with the cylindrical axis perpendicular to the foliation of the rock.

For monochromatic radiation, selected pole figures were extracted and then processed with Beartex [13] to obtain an orientation distribution (OD). From the OD, selected pole figures were calculated.

Texture analysis from TOF-diffraction spectra was done using the software package MAUD (Materials Analysis Using Diffraction) [15], relying on the Rietveld method, refining texture, structural parameters, phase quantities, and crystallite size. MAUD is a Java-based program, which allows it to be run on a variety of computing platforms.

For texture calculations, both procedures used the WIMV algorithm, a discrete method based on tomographic principles [16]. After the MAUD refinement, orientation distributions are exported and used in BEARTEX to calculate and plot pole figures [13]. Texture of feldspars (plagioclase and orthoclase) was found to be minimal, consistent with previous studies [9, 17], and are not considered further.

It should be mentioned that for biotite, monochromatic radiation is preferred because main diffraction peaks of interest are at high d-spacings, where counting statistics for TOF is very poor, even for low-angle detectors.

Results

Preferred orientation

Samples PC 708, 709, 714, 715, 718, and 720 were used for TOF neutron texture analysis. PC 82, 89, and 92 were measured with monochromatic neutrons [9]. Figure 2 displays pole figures for quartz (a) and biotite (b) for typical samples in order of increasing deformation.

Biotite preferred orientation continues to strengthen with increasing deformation from a maximum of 1.4 m.r.d. in weakly deformed granite (PC 715) to 12 m.r.d. in phyllonite (PC 92) [9]. (001) lattice planes become aligned in the schistosity plane with some bending around the lineation direction. Quartz preferred orientation also increases in strength as granite deforms to mylonite, with a c-axis maximum in the intermediate fabric direction Y (in the schistosity plane and perpendicular to lineation). This is a typical pattern in recrystallized quartzites and is regionally observed in Santa Rosa mylonites [17]. The maximum increases from 1.5 (PC 715) to 5.5 m.r.d. (PC 82). With further deformation and grain size reduction, quartz textures attenuate and randomize in phyllonite. Different mechanisms become active, for example grain boundary sliding.

Microstructure

Determinations of dislocation density for granite came from samples PCs 89 and 715, for mylonite came from PCs 708, 709, 714, and 720, and for phyllonite from PC 92 and 718. The number of images captured was 20 of granite, 36 of mylonite, and 70 of phyllonite. Images were taken at different magnifications, depending on grain size and dislocation densities. The average dislocation density in quartz from each rock type is listed in Table 4.

Fig. 2 Pole figures for selected samples from the Santa Rosa mylonite zone, calculated from the orientation distribution based on neutron diffraction data, in order of increasing deformation. The pole figures for quartz 0001 (**a**) and biotite 001 (**b**) are projected onto the foliation plane, the macroscopic lineation is X, and the intermediate direction is Y. Linear contour scale (in multiples of a random distribution, m.r.d.), equal area projection
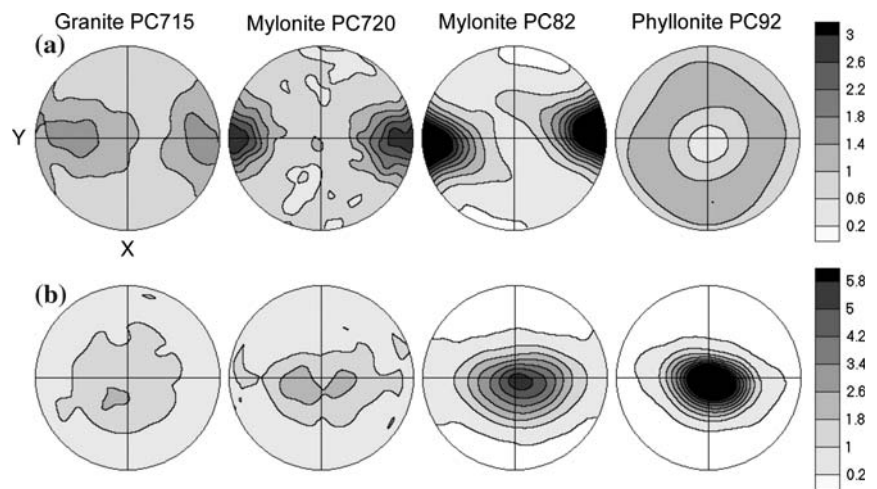
Table 4 The average dislocation densities of each rock type are calculated from 20 granite, 36 mylonite, and 70 phyllonite images

Rock type	Average dislocation density (dislocations/cm^2)	Range
Granite	7.1×10^7, std 3.2×10^7	3.1×10^7 to 1.3×10^8
Mylonite	2.3×10^8, std 6.8×10^7	1.0×10^8 to 3.3×10^8
Phyllonite*	Both high and low density regions	2.6×10^7 to $\sim 10^9$

* Many images were uncountable due to high dislocation densities. Although some images for phyllonite contained low densities, a majority of the images showed high dislocation densities and the average would be considered close to 10^9

Dislocation density for each image was obtained by first counting the number of dislocation ends present. The number of dislocation ends was then divided in half, which is now equivalent to the number of dislocations present in the image. The area of the image, which can be calculated from the magnification, then divides the number of dislocations yielding the dislocation density. Representative images of quartz grains are shown for rocks that were classified as granite in Fig. 3a, b, mylonite in Fig. 3c, d, and phyllonite in Fig. 3e, f.

The average dislocation densities given in Table 4 show that on average mylonite has approximately 3 times more dislocations per unit area than granite. With the understanding that Santa Rosa mylonites form predominantly by ductile deformation of granite, this comes as no surprise [7–10]. The dislocation densities found in these rocks are in agreement with other studies of deformed granitic rocks, and naturally or synthetically deformed quartz, which have been found to have dislocation densities in the range of 10^5 to 10^{12} cm^{-2} [18–20].

As mylonite deforms and becomes phyllonite, dislocation densities continue to increase, and in some cases, form dense tangles of dislocations, as shown in Fig. 3e. The

increase in dislocations also means that the strain energy of quartz becomes higher. In order to lower the energy state of the grain, dislocations move into preferred arrangements by recovery, forming boundary walls. These walls divide the crystal into sub-grains, concentrating dislocations in walls, while leaving the bulk of the sub-grain depleted in dislocations, as shown in Fig. 3f.

Expansion tests

The results of ASTM C 1260 are shown in Fig. 4 for samples PC 89, 92, 708, 709, 714, 715, 718, and 720. The results indicate that expansion of mortar bars increases from granite to mylonite to phyllonite when these rocks are used as aggregate.

Discussion

The effect of dislocations on the reactivity of quartz has been estimated by calculating the increase in internal energy of quartz with varying dislocation density. The strain energy in a crystal lattice caused by dislocations can be described using ideal elastic behavior [20–23]. The increase in the internal energy of quartz caused by dislocations can be calculated by the following equation [20]:

$$\Delta E = D \left(\frac{\mu b^2}{8\pi K} \right) \ln \left(\frac{r_{\mathrm{h}}^2 + d^2}{r_{\mathrm{h}}^2} \right) \qquad (1)$$

with

$$r_{\mathrm{h}}^2 = \frac{\mu b^2 V}{8\pi^2 K \, \Delta H_{\mathrm{m}}}$$

where D is the dislocation density (cm^{-2}); μ is the shear modulus (4.44×10^{11} dyne cm^{-2}) [24]; v is the Poisson's

Fig. 3 Brightfield TEM images of dislocation structures in quartz. (**a**) PC 89, granite. Two quartz grains containing dislocations separated by a grain boundary (seen running diagonally from top left to bottom right). The width of the image is 9.7 μm and the dislocation density is 7×10^7 dislocations cm^{-2}. (**b**) PC 715, granite. The width of the image is 8.4 μm and the dislocation density is 9.6×10^7 dislocations cm^{-2}. (**c**) and (**d**) PC 708, mylonite. (**c**) Image width is 5.7 μm, and the dislocation density is 1.6×10^8 dislocations cm^{-2}. (**d**) Image width is 4 μm, and the dislocation density is 2.8×10^8 dislocations cm^{-2}. (**e**) and (**f**) PC 92, phyllotite. (**e**) The high density of dislocations produces tangles. The width of the image is 4 μm. (**f**) Some dislocations arranged to form a sub-grain boundary. The width of the image is 2 μm
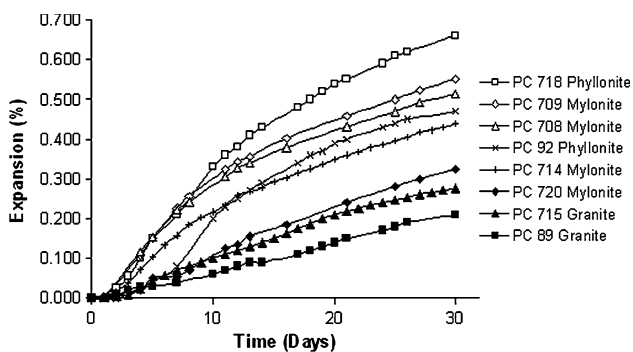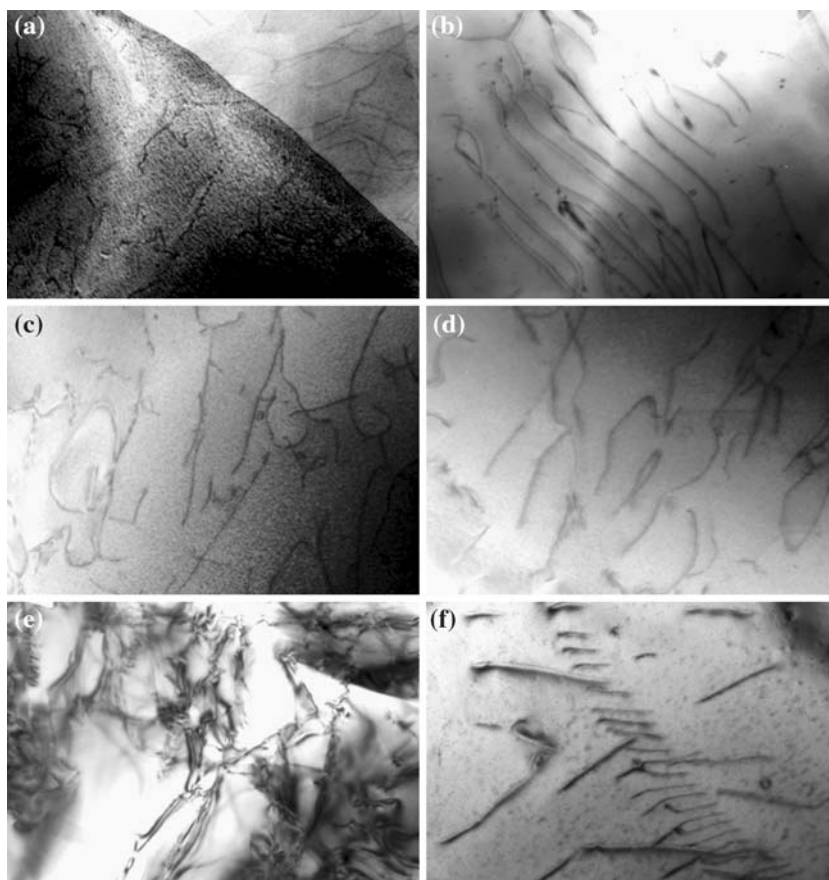
Fig. 4 Plot of reactivity of aggregates as determined by ASTM C 1260 showing expansion in percent versus time in days

ratio (0.077) [24]; V is the molar volume (22.688 cm^3 mol^{-1}) [25]; ΔH_m is the enthalpy of melting (8.159 kJ mol^{-1}) [25]; b is the magnitude of the Burgers vector (4.913–7.304 Å) [24]; d is the mean distance between dislocations $(1/D)^{1/2}$; and K is a constant related to the Burgers vector orientation, where $K = 1$ for a screw dislocation and $K = 1 - v$ for an edge dislocation, where v is Poisson's ratio.

The internal energy is also dependent on the orientation of the dislocation relative to the Burgers vector. Equation 1 assumes that the dependence is small, and is represented by

the constant K [26]. Substituting the values into Eq. 1, the increase in energy of quartz caused by a particular dislocation density on a particular slip system containing a certain type of dislocation can be calculated. Table 5 shows the calculated change in energy of quartz with varying dislocation density. It can be seen that even when the parameters that created the maximum change in energy are used, the energy is still small. Even for a dislocation density as high as 10^{11}, the energy contributed to quartz is only 6% of the dissolution energy (assuming 2.3 kJ/mol).

Dislocations may not contribute much to the bulk energy increase of quartz, but they may nevertheless affect the reactivity of quartz by providing favorable areas for chemical processes such as precipitation and dissolution to occur. The addition or removal of the first few atoms on an atomistically flat surface results in a large change in the

Table 5 Calculated changes in the internal energy (ΔE) of quartz at varying dislocation densities assuming screw dislocations on the $\langle a \pm c \rangle$ slip system

Dislocation Density (cm^{-2})	1×10^8	1×10^9	1×10^{10}	1×10^{11}
ΔE (J mol^{-1})	0.15	2.50	20.08	151.60
%Dissolution energy	6.5×10^{-3}%	0.11%	0.87%	6.51%

surface area, and thus a large change in the surface free energy. Once the addition or removal area exceeds a critical radius, the change in surface energy decreases, allowing for a more thermodynamically favorable reaction. Dislocations, specifically screw dislocations, provide an unending source of steps for precipitation and dissolution reactions to occur [27]. This spiral crystal model has been observed to control quartz growth and dissolution, with equal efficiency during both growth and dissolution [28–30].

Another contribution of dislocations is the strain energy associated with them. It has been recognized that, although the strain energy of dislocations contributes only a small amount to the total internal energy of quartz crystals, the strain energy is more concentrated around the dislocations themselves, and is not distributed through the bulk crystal. It has been suggested that a large amount of strain energy is released during dissolution such that it decreases or eliminates the energy barrier (caused by the change in free surface energy) that prevents the removal of atoms. This may lead to regions of quartz where the reactivity is enhanced, potentially allowing reactions other than dissolution to occur at higher rates [20, 31–34].

An increase by 2–3 orders of magnitude in dislocation density has been shown to increase the dissolution rate by as much as a factor of 3 [35–41]. Therefore, quartz grains containing higher dislocation densities due to deformation may be a contributing factor leading to an enhancement of the susceptibility to the alkali-silica reaction when compared to quartz grains that have lower dislocation density and undergone less deformation.

Table 6 lists the rock type, the average expansion of each rock type using ASTM C 1260, and the average dislocation density of each type. Expansion values from ASTM C 1260 were taken at 30 days.

Figure 5 is a plot of the data in Table 6, showing the log of the average dislocation density versus the average expansion percentage. This plot illustrates the positive correlation between expansion, which is an indicator of reactivity, with dislocation density. This would suggest that dislocations have a strong effect on the reactivity of quartz bearing rocks with respect to the ASR.

While the observation of dislocations in quartz grains using TEM and the measurement of dislocation densities may provide a quantitative means to define the reactivity of a rock, this method is very laborious and painstaking, requiring a large amount of time for preparation, analysis, and image processing. In most cases, this process is not suitable for quick and easy determination of aggregate reactivity. Texture analysis of the preferred orientation of mineral grains within these deformed rocks may provide a suitable alternative to assess the deformation state of a rock, though obviously there is no direct relationship between biotite preferred orientation and dislocation densities in quartz.

Figure 5 also shows a plot of the quartz (0001) pole figure maxima versus the expansion % illustrating that no linear correlation exists between quartz texture and susceptibility to the alkali-silica reaction. Quartz texture increases during initial deformation. However, a change in the mechanism of stress accommodation at high deformation causes the preferred orientation of quartz to be destroyed [8, 9, 42, 43].

Unlike quartz, biotite texture increases with deformation. In Fig. 5, a plot of the biotite (001) pole figure maximum versus expansion %, suggests a monotonic relationship between biotite texture and the susceptibility of quartz grains within the same rock to the alkali-silica reaction. Even though biotite is not a reactant in the alkali-silica reaction, it is commonly present in granitic rocks as
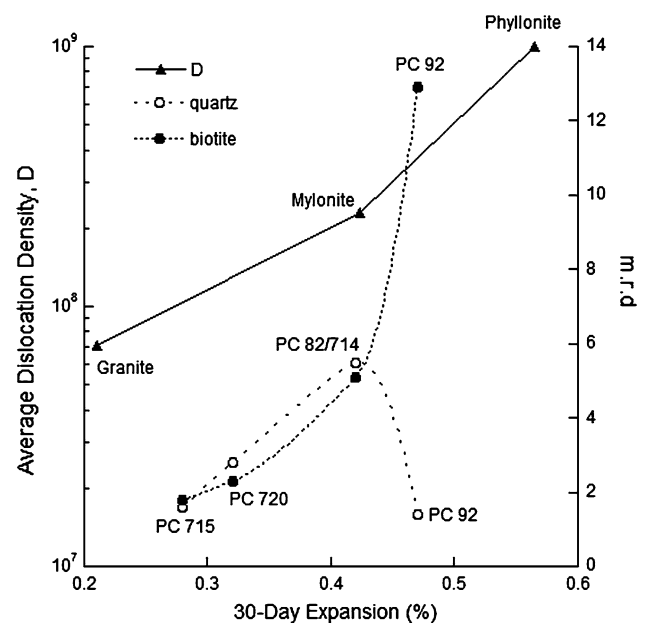
Fig. 5 Plot of the average 30-day expansion value of each rock type from ASTM C 1260 tests versus log of its corresponding dislocation density D as taken from Table 4 and (001) pole figure maximum for quartz and biotite in multiples of a random distribution (m.r.d)

Table 6 The average expansion and average dislocation density of each rock type

Rock type	30-Day expansion (%)	Dislocation density (cm^{-2})
Granite	0.210	7.1×10^7
Mylonite	0.424	2.3×10^8
Phyllonite	0.565	$\sim 10^9$

an accessory mineral. Biotite texture may indicate quartz susceptibility to the alkali-silica reaction.

Summary

TEM images of quartz grains in deformed granitic rocks show an increase in dislocation density with increasing deformation. The susceptibility to the alkali-silica reaction of these rocks used as aggregate in concrete may be estimated from the amount of expansion using a standardized test known as ASTM C 1260. Using expansion testing as an estimate for the reactivity of quartz, a comparison was made to the dislocation density of each rock type. It was shown that a positive correlation exists between the expansion and dislocation density, suggesting that dislocations might play a major role in determining the reactivity of quartz bearing rocks with respect to the alkali-silica reaction.

Neutron diffraction texture analysis shows that for quartz, there is no simple relationship between preferred orientation and the susceptibility to the alkali-silica reaction. However, textures of biotite, a common accessory mineral in granite, reveal a linear relationship with reactivity. These results suggest that preferred orientation of biotite may be used to estimate the deformation state of the rock and thus, susceptibility of rocks containing both biotite and quartz to the alkali-silica reaction. Clearly grain size also is an important factor.

References

1. Gogte BS (1973) Eng Geol 7:135
2. Grattan-Bellew PE (1986) Proceedings of the 7th international conferenc on alkali-aggregate reaction. Park Ridge, NJ, p 434
3. Grattan-Bellew PE (1992) Proceedings of the 9th international conference on alkali-aggregate reaction in concrete, Concrete Society Publication CS 104, vol 1. London, p 383
4. French WJ (1992) Proceedings of the 9th international conference on alkali-aggregate reaction in concrete, Concrete Society Publication CS 104, vol 1. London, p 338
5. Kerrick DM, Hooton RD (1992) Cement Concrete Res 22:949
6. Monteiro PJM, Shomglin K, Wenk H-R, Hasparyk NP (2001) ACI Mater J 98:179
7. Wenk H-R (1998) J Struct Geol 20:559
8. Goodwin LB, Wenk H-R (1995) J Struct Geol 17:689
9. Wenk H-R, Pannetier J (1990) J Struct Geol 12:177
10. O'Brien DK, Wenk H-R, Ratschbacher L, You Z (1987) J Struct Geol 9:719
11. Hutchison CS (1975) Schweizerische Mineralogische und Petrographische Mitteilungen 55:243
12. American Society for Testing and Materials (2002) Standard test method for potential alkali reactivity of aggregates (Mortar-Bar method), ASTM C 1260-01, Annual book of ASTM standards, vol 04.02. American Society for Testing and Materials, Philadelphia
13. Wenk H-R, Matthies S, Donovan J, Chateigner D (1998) J Appl Crystallogr 31:262
14. Wenk H-R, Lutterotti L, Vogel S (2003) Nucl Instr Methods A 515:575
15. Lutterotti L, Matthies S, Wenk H-R (1999) Int U Crystallogr Comm Powder Diffr Newsl 21:14
16. Matthies S, Vinel G (1982) Phys Status Solidi B 112:K111
17. Pehl J, Wenk H-R (2005) J Struct Geol 27:1741
18. Anderson GM, Burnham CW (1965) Am J Sci 263:494
19. Liddell NA, Phakey PP, Wenk H-R (1976) In: Wenk H-R (ed) Electron microscopy in mineralogy. Springer Verlag, Heidelberg, p 419
20. Blum AE, Yund RA, Lasaga AC (1990) Geochim Cosmochim Acta 54:283
21. Van Der Hoek B, Van Der Eerden JP, Bennema P (1982) J Cryst Growth 56:621
22. Hirth JP, Lothe J (1982) Theory of dislocations. John Wiley and Sons, New York
23. Wintsch RP, Dunning J (1985) J Geophys Res 90:3649
24. Heinisch HL, Sines G, Goodman JW, Kirby SH (1975) J Geophys Res 80:1885
25. Robie RA, Hemingway BS, Fisher JR (1978) United States Geological Survey Bulletin 1452
26. Lasaga AC, Blum AE (1986) Geochim Cosmochim Acta 50:2363
27. Somorjai GA (1994) Introduction to surface chemistry and catalysis. John Wiley and Sons, New York
28. Zimonyi G (1957) Acta Phys Hungaria 8:119
29. Augustine F, Hale DR (1960) J Phys Chem Solids 13:344
30. Burton WK, Cabrera N, Frank FC (1951) Philos Trans R Soc London A 243:299
31. Cabrera N, Levine MM (1956) Philos Mag 1:450
32. Lasaga AC (1983) Proceedings of the 4th international symposium on water–rock interactions, p 269
33. Brantley SL, Crane SR, Credar DA, Hellmann R, Stallard R (1986) Geochim Cosmochim Acta 50:2349
34. Brantley SL, Crane SR, Credar DA, Hellmann R, Stallard R (1986) Geochem Process Miner Surf. In: Davis JA, Hayes KF (eds) Amer Chem Soc Symposium Series 323. Washington DC, p 634
35. Murr LE, Hiskey JB (1981) Metall Trans 12B:255
36. Casey WC, Carr MJ, Graham RA (1988) Geochim Cosmochim Acta 52:1545
37. Holdren GR, Casey WH, Westrich HR, Carr M, Boslough M (1988) Chem Geol 70:79
38. Schott J, Brantley S, Credar D, Guy C, Borcsik M, Willaime C (1989) Geochim Cosmochim Acta 53:373
39. Blum AE, Lasaga AC, Yund RA (1990) Geochim Cosmochim Acta 54:283
40. Gratz AJ, Bird P, Quiro GB (1990) Geochim Cosmochim Acta 54:2911
41. Liu M, Yund RA, Tullis J, Toper L, Navrotsky A (1995) Phys Chem Minerals 22:67
42. Boullier AM, Guegen Y (1975) Contrib Mineral Petrol 23:128
43. Behrmann JH, Mainprice D (1997) Tectonophysics 140:297